Structure
Article

Partial Agonists Activate PPARγ Using a Helix 12 Independent Mechanism

John B. Bruning,[1] Michael J. Chalmers,[2] Swati Prasad,[2] Scott A. Busby,[2] Theodore M. Kamenecka,[3] Yuanjun He,[3] Kendall W. Nettles,[1,*] and Patrick R. Griffin[2,*]
[1]Department of Cancer Biology
[2]Department of Molecular Therapeutics
[3]Department of Medicinal Chemistry
The Scripps Research Institute, 5353 Parkside Drive, Jupiter, FL 33458, USA
*Correspondence: knettles@scripps.edu (K.W.N.), pgriffin@scripps.edu (P.R.G.)
DOI 10.1016/j.str.2007.07.014

SUMMARY

Binding to helix 12 of the ligand-binding domain of PPARγ is required for full agonist activity. Previously, the degree of stabilization of the activation function 2 (AF-2) surface was thought to correlate with the degree of agonism and transactivation. To examine this mechanism, we probed structural dynamics of PPARγ with agonists that induced graded transcriptional responses. Here we present crystal structures and amide H/D exchange (HDX) kinetics for six of these complexes. Amide HDX revealed each ligand induced unique changes to the dynamics of the ligand-binding domain (LBD). Full agonists stabilized helix 12, whereas intermediate and partial agonists did not at all, and rather differentially stabilized other regions of the binding pocket. The gradient of PPARγ transactivation cannot be accounted for solely through changes to the dynamics of AF-2. Thus, our understanding of allosteric signaling must be extended beyond the idea of a dynamic helix 12 acting as a molecular switch.

INTRODUCTION

Peroxisome proliferator-activated receptors (PPARs) belong to the nuclear receptor superfamily of transcription factors, acting as obligate heterodimers with the retinoid X receptor (RXRα, β, and γ) to control genes implicated in energy, carbohydrate, and lipid metabolism (Berger and Wagner, 2002; Chawla et al., 2001). These heterodimeric transcriptional complexes can be activated by agonists of either PPAR or RXR such as eicosanoids, prostaglandins, retinoic acids, and synthetic agonists, allowing the integration of transcriptional responses from two distinct ligand-regulated signaling pathways (Forman et al., 1995; Gottlicher et al., 1992; Kliewer et al., 1997, 1992).

One important class of synthetic agonist of peroxisome proliferator-activated receptor gamma (PPARγ) is the thiazolidinediones (TZDs) (e.g., rosiglitazone and pioglitazone) (Greene, 1999). TZDs are antidiabetic agents that target adipose tissue and improve insulin sensitivity through pleiotropic effects (Day, 1999; Pearson et al., 1996). Despite the clinical benefit of these drugs, use of TZDs has been associated with adverse effects including weight gain, increased adipogenesis, renal fluid retention, and plasma volume expansion and, more recently, possible increased incidence of cardiovascular events (Berger et al., 2005; Nissen and Wolski, 2007). It is interesting to note that the structurally similar PPARγ TZD full agonists rosiglitazone (Avandia) and pioglitazone (Actos) afford different clinical adverse events. This indicates that subtle changes in ligand receptor interaction lead to differences in the pharmacology of these agents, highlighting the importance of the need for a more complete understanding of the mechanism of ligand modulation of PPARγ.

As a result of the clinical observations mentioned above, emphasis has shifted to the development of "selective PPARγ modulators" or SPPARMs. SPPARMs are PPARγ modulators that exhibit potent insulin sensitization activity but are antiadipogenic in animal models of type 2 diabetes (Berger et al., 2003; Rangwala and Lazar, 2002; Rocchi et al., 2001). Partial agonists display reduced transcriptional activity in reporter assays and, in animal models of type 2 diabetes, they demonstrate the SPPARM phenotype.

Selective recruitment of transcriptional coactivators has been implicated in partial agonist and SPPARM phenotype. The binding of agonist to the receptor's LBD induces structural changes that facilitate dissociation of repressor molecules (e.g., NCoR and SMRT) and association of activator proteins (Nagy et al., 1999; Shiau et al., 1998). These transcriptional coactivators bind to the receptor complex, modify local chromatin structure, and recruit the transcription machinery to target gene promoters (Rosenfeld et al., 2006). Partial agonists have been shown to have decreased recruitment of CBP and SRC1 coactivators (Fujimura et al., 2005) but retain association with PGC1α (Burgermeister et al., 2006).

Significant effort has been placed on dissecting the mechanism of ligand activation of PPARγ. Based on previous studies, it has been suggested that communication between ligand and coregulator binding sites occurs

through a molecular switch comprised of the most carboxy terminal helix, H12 of the LBD (Nagy and Schwabe, 2004; Rosenfeld et al., 2006). Full agonist ligands contact PPARγ H12, stabilizing the agonist conformation through a direct hydrogen bond to Tyr473, allowing H12 to dock against H3 and H11 (Nolte et al., 1998). In this conformation, H12 forms part of the coactivator-binding site (AF-2 surface), along with H3-5. Antagonists physically obstruct the agonist conformation of H12 through a bulky pendant group that protrudes from within the ligand-binding pocket or, in the case of the antagonist GW-9662, which covalently modifies Cys313 similar to the partial agonist L-764406, blocks agonist binding (Bendixen et al., 2001; Elbrecht et al., 1999; Shiau et al., 1998).

Previous X-ray crystallographic studies have revealed that agonist-bound and apo PPARγ LBDs are largely conserved with no global differences. The large similarity of apo, full-agonist-, and partial-agonist-bound structures lead to the hypothesis that differences in ligand binding modes were controlled largely by dynamics, particularly H12 and the AF-2 surface. The structure of a partial-agonist-bound PPARγ showed no direct interactions between ligand and H12 (Oberfield et al., 1999), supporting the idea that this structural feature is key to maximal transactivation potency. This model is further supported by fluorescence labeling of H12 (Kallenberger et al., 2003), which demonstrated that full agonists stabilize PPARγ H12. These studies implicated that the degree of H12 stabilization is proportional to the degree of agonism and transcriptional output for full agonists. However, these studies did not examine partial agonist interactions and were designed such that they could only examine the dynamics of H12.

Amide hydrogen/deuterium exchange (HDX) is an established technique for measuring protein dynamics (Englander, 2006; Maier and Deinzer, 2005; Shi et al., 2006). In contrast to fluorescence labeling methods, no prior modification of the protein of interest is required and kinetic information may be obtained across the entire protein. Previously, Yan and colleagues utilized HDX to probe conformational dynamics of the retinoid X receptor alpha LBD (RXRα LBD) in the presence and absence of 9-*cis*-retinoic acid (9-*cis*-RA) (Yan et al., 2004). In that study, perturbation in HDX kinetics of RXRα LBD upon 9-*cis*-RA binding correlated well with changes in hydrogen bonding, amino acid residue depth, and solvent exposure predicted from the cocrystal structure. However, perturbation in exchange kinetics was also observed in regions not predicted from the X-ray structure. Yan's work illustrates the complementary relationship between HDX kinetics and X-ray crystallography and demonstrates the ability of HDX to detect allosteric effects on dynamics as a result of ligand binding.

We recently presented the first HDX study of PPARγ bound to a molecule with a low transactivation potential (partial agonist) and found no changes in the dynamics of H12 as compared to the apo receptor (Hamuro et al., 2006). Selective loss of coactivator recruitment with partial agonists was hypothesized to derive from lack of stabilization of the coactivator-binding site AF-2. This supports a model whereby stabilization of H12 correlates with full transcriptional activity; however, the model could not explain the transactivation activity of partial agonists that do not stabilize H12 at all. More importantly, previous studies cannot explain the activity of intermediate agonists such as BVT.13, which affords transactivation potential twice that of partial agonists and yet BVT.13 makes no direct hydrogen bond to H12 (Ostberg et al., 2004).

In this study, we sought to determine how ligands of PPARγ can afford graded transcriptional responses in the absence of H12 stabilization. We extended our previous studies by coupling HDX analysis with X-ray crystallographic studies to profile a series of agonists that afford graded transcriptional activation. Ligands included two full agonists (>80% TA as compared to rosiglitazone), three partial agonists (<50% TA), and a compound with intermediate transactivation (between 50% and 80% TA). Recent improvements in our HDX platform facilitated rapid, robust, and quantitative assessment of amide HDX for the entire receptor LBD (Chalmers et al., 2006). HDX kinetics of H12 was altered only in the presence of full agonists such as rosiglitazone. Analysis of partial agonists and the intermediate agonist BVT.13 demonstrated that the dynamics of H12 was unaltered by these ligands. Thus, H12 cannot control activation of the receptor by agonists with transactivation activation below 80% as compared to rosiglitazone. In addition to differences in H12 stabilization, the intermediate and partial agonists demonstrated statistically significant protection to exchange in the β sheet region of the receptor. In order to better understand the molecular details that underlie this novel structural feature, we obtained six crystal structures of PPARγ bound to the ligands described above. The full agonist afforded the expected hydrogen bond directly to H12; however, the remaining ligands demonstrated interactions with the β sheet, revealing a structural feature that can be exploited by high-affinity intermediate and partial agonists.

In summary, these data refute the hypothesis that the dynamics of H12 is the only mediator of graded transcriptional responses. We also demonstrate that other structural features such as the β sheet region of PPARγ are important in ligand-specific activation of the receptor, and these regions likely represent novel interaction sites for coactivators. These studies highlight the power of combining crystallographic studies with comprehensive HDX profiling, and the results presented provide novel insight into the mechanism of ligand activation of nuclear receptors.

RESULTS

Agonists Display a Wide Gradient of Transcriptional Activation

We assembled a small collection of PPARγ modulators, most of which were previously described in the literature (Figure 1A). These ligands demonstrated varying potency in a FRET-based HTRF assay and afforded graded

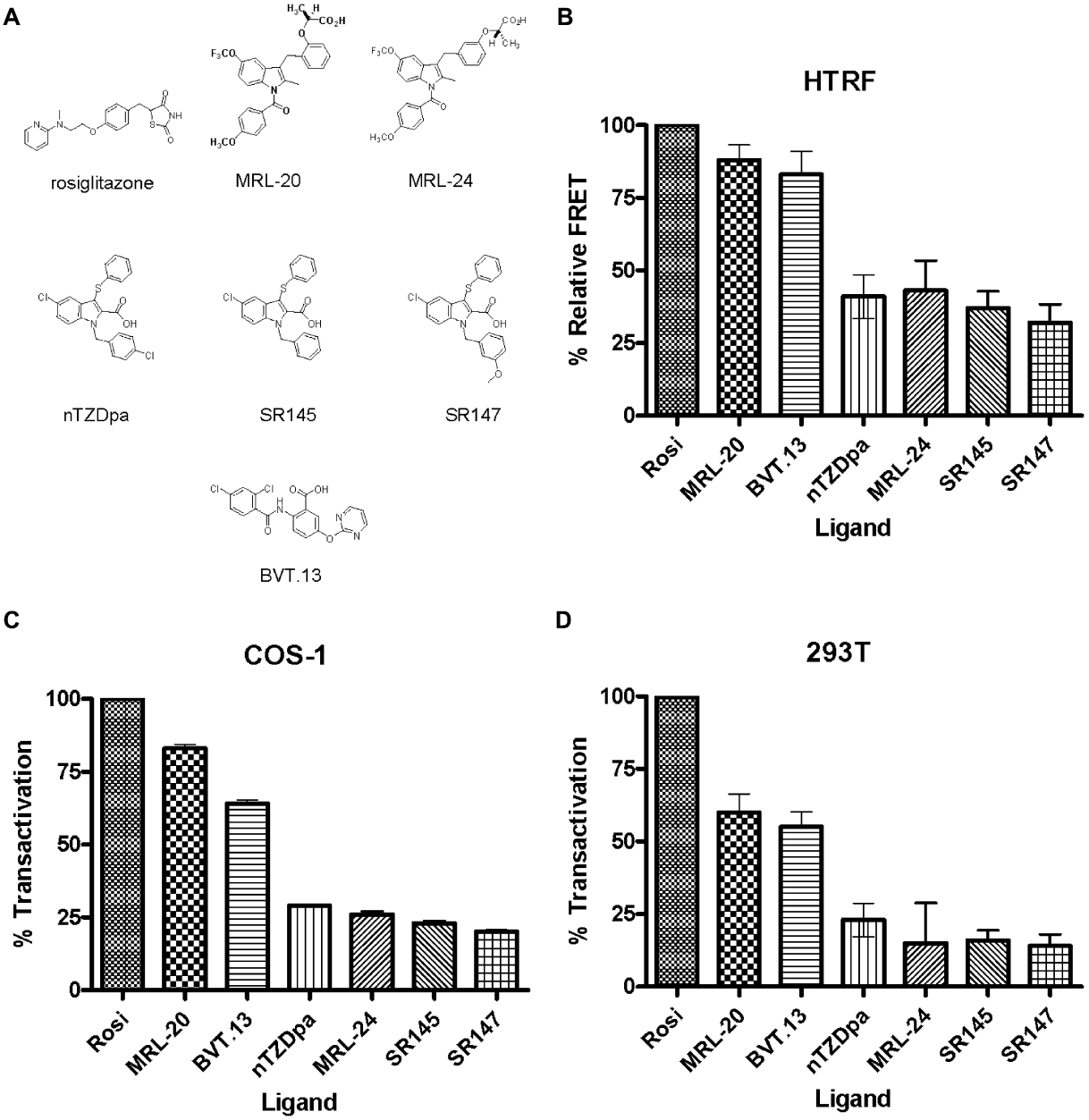

Figure 1. PPARγ Ligands and Graded Transcriptional Responses

(A) Chemical structures of the ligands.

(B) Relative FRET for the indicated compounds in a HTRF-based assay.

(C) Cos-1 cells were transfected in triplicate with a PPARγ expression vector and DR-1-luciferase reporter for 24 hr with the indicated compounds.

(D) Human 293T cells were transfected in triplicate with a PPARγ expression vector and PPREX3-luciferase reporter for 24 hr with the indicated compounds. Error bars represent the standard deviation around the mean value where n = 3.

transcriptional responses in a cell-based luciferase reporter assay similar to that previously described with a few modifications (Figures 1B–1D) (Berger et al., 2003). Two of these compounds, MRL-24 and nTZDpa, are high-affinity partial agonists that afforded low levels of transactivation activation (Figures 1C and 1D), consistent with previous reports (Acton et al., 2005; Berger et al., 2003). These compounds represent important chemical probes because of their desired pharmacological profile in animal models of type 2 diabetes such as the diet-induced obese mouse or the leptin-receptor-impaired *db/db* mouse models, where these compounds improve insulin sensitization in the absence of weight gain, plasma volume expansion, or increased heart weight (Acton et al.,

2005; Berger et al., 2003). In order to expand the nTZDpa series, we synthesized SR145 and SR147, which displayed similarly modest transactivation profiles (Figures 1C and 1D). The partial agonist MRL-24 is a regioisomer of the full agonist MRL-20, differing only by meta versus ortho placement of the lactate group, providing a matched set of ligands for structural comparison. Lastly, we examined the PPARγ ligand BVT.13, which in previous crystallographic studies (Ostberg et al., 2004) was shown to not interact with H12. This ligand demonstrates intermediate transcriptional efficacy (~60% relative to rosiglitazone, Figures 1C and 1D). As described below, the X-ray crystal structure revealed that nTZDpa binds very similarly to BVT.13, but they displayed divergent transactivation profiles, again providing a matched set of compounds for structural comparison.

Structure Determination

PPARγ LBD was crystallized alone and ligands were soaked into apo crystals. The phase problem was solved by molecular replacement and the resolution of six ligand bound structures ranged from 2.05–2.40 Å (Table 1). The structures revealed the canonical nuclear receptor tertiary fold, comprised of three layers of α helices and a four strand β sheet (Figure 2A). The PPARγ LBD asymmetric unit contained one dimer, with nearly identical monomers. In each of the structures, H12 was distorted in one of the monomers due to crystallographic contacts, consistent with previously published PPARγ structures (Cronet et al., 2001; Ebdrup et al., 2003; Nolte et al., 1998; Oberfield et al., 1999; Sauerberg et al., 2002). The overall structure of the PPARγ LBD remained largely unchanged among these six ligand-bound receptor complexes and all structures showed a strong overall agreement with rosiglitazone-bound PPARγ, with rmsd values ranging from 0.64–0.81 Å for superimposed alpha carbons (Figure 2B).

Composite omit $2f_o$-f_c difference maps for the observed structures revealed clear and unambiguous density for all of the ligands (Figures 3A–3F). Previously, the structure of the intermediate agonist BVT.13 bound to PPARγ LBD and a coactivator peptide was reported (Ostberg et al., 2004). The structure presented here (Figure 3F) was obtained in absence of a coactivator peptide and was solved at a resolution 0.5 Å higher than the one reported previously. Our structure revealed water molecules in the binding pocket that make contacts with the intermediate agonist. Also presented here is the structure of PPARγ bound to the partial agonist nTZDpa (Figure 3C), which occupies a similar location in the ligand binding pocket as the intermediate agonist BVT.13. Two analogs of nTZDpa, SR145 and SR147, are also reported (Figures 3D and 3E); finally, structures of two regioisomers MRL-20 (full agonist) and MRL-24 (partial agonist) are shown in Figures 3A and 3B.

Hydrogen/Deuterium Exchange of PPARγ LBD

To understand the role of dynamics in mediating agonist activity, we performed comprehensive differential HDX experiments on the following ligand-receptor complexes: PPARγ LBD ± rosiglitazone, MRL-20, MRL-24, nTZDpa, and BVT.13. HDX analysis of SR145 and SR147 was not performed as these ligands demonstrated equivalent transactivation activation as the precursor compound nTZDpa. Each differential HDX experiment measured exchange kinetics of 27 different regions of the receptor LBD. For each of the 27 regions of the receptor, a comparison was made between the exchange kinetics of the apo receptor to that of ligand-bound receptor. The reduction in HDX kinetics for each region of the receptor following ligand interaction is detailed in Figure 4. Figure S1 (see the Supplemental Data available with this article online) shows the underlying %D versus Log time plots for every peptide in the dataset. Improvements to our HDX platform since our previous work on PPARγ, such as the inclusion of a 1 s on-exchange time point, allowed us to accurately measure HDX of highly dynamic regions of the receptor. More importantly, the implementation of parallel analysis of an apo-receptor sample for each ligand complex, coupled with a randomized order of analysis, eliminated systematic errors and improved our ability to observe subtle changes in receptor dynamics.

As shown in Figure 5, the apo receptor demonstrated a build-up of deuterium in H12 (residues 470–477) that saturated by 30 s. The full agonists rosiglitazone and MRL-20 significantly reduced the rate of amide exchange kinetics for H12. However, no statistically significant stabilization of H12 was observed for either the partial agonist MRL-24 and nTZDpa or the intermediate agonist BVT.13. The β sheet region (amino acids 341–351) is another area of receptor that demonstrates differential HDX following ligand binding (Figure 4 and Figure 5). Full agonists showed moderate stabilization of this region. In contrast, MRL-24, nTZDpa, and BVT.13 induced robust protection from exchange in this region. As discussed below, the crystal structures identified a hydrogen bonding network between these ligands and the β sheet that was not found with the full agonists. Figure 6 illustrates how HDX kinetics in H12, β sheet, and H3 correlate with transactivation efficacy. The activity of BVT.13 is completely independent of H12, and there is an apparent compensation of β sheet stabilization as H12 stabilization is decreased (Figure 6B). The putative structural features governing this phenomenon are described below.

Intermediate and Partial Agonism Does Not Correlate with Stabilization of H12

The full agonists rosiglitazone and MRL-20, when bound to receptor, induced a statistically significant reduction in the rate of amide exchange kinetics for H12. In addition, the degree of stabilization of H12 was consistent with the degree of transactivation for these full agonists. Full agonist MRL-20 shows 20% less transactivation compared to rosiglitazone while also showing a lower degree of H12 stabilization compared to rosiglitazone (Figure 6A). As described above, no statistically significant stabilization of H12 was observed for either partial agonist MRL-24 or nTZDpa. More importantly, stabilization of H12

Table 1. Summary of Crystallographic Statistics

	BVT.13	MRL-24	SR147	MRL-20	nTZDpa	SR145
Data Collection						
Beamline	APS SER-CAT	APS SER-CAT	APS SER-CAT	SSRL BL1-11	SSRL BL1-11	SSRL BL-1-11
Wavelength (Å)	0.9764	0.9764	0.9764	0.9537	0.9537	0.9537
Space group	C2	C2	C2	C2	C2	C2
Unit cell parameters (Å)						
a	92.3	91.4	90.8	89.2	89.7	90.1
b	62.0	61.5	62.3	63.9	62.2	62.4
c	118.1	117.9	118.1	119.2	118.0	117.9
Unique angle (°) β	102.3	102.4	101.1	103.4	101.0	101.0
Resolution (Å)	15–2.4	15–2.3	15–2.4	15–2.2	15–2.05	15–2.2
Unique reflections	20,711	24,664	21,496	31,004	34,179	35,178
Average redundancy	6.3 (4.0)	6.3 (4.4)	6.3 (3.3)	6.8 (4.3)	6.9 (4.4)	7.1 (6.7)
Completeness (%)[1]	91.4 (59.1)	91.7 (63.5)	91.3 (56.8)	99.2 (99.2)	99.3 (95.3)	99.4 (99.6)
R_{merge}[2]	0.056 (0.173)	0.049 (0.119)	0.068 (0.196)	0.073 (0.42)	0.055 (0.34)	0.066 (0.42)
I/σ	26.8 (7.6)	25.4 (10.4)	24.6 (4.8)	23.1 (2.9)	33.4 (3.4)	30.2 (4.7)
Refinement						
Resolution (Å)	2.4	2.3	2.4	2.2	2.05	2.2
R_{free}[3]/R_{work}[4]	26.4/20.6	24.7/20.6	28.4/26.9	23.0/18.0	24.5/19.7	23.5/19.6
Average B factor (Å^2)						
Protein	39.58	43.81	90.21	21.99	23.86	22.59
Ligand	68.33	63.42	70.17	33.19	33.796	34.23
Water	66.56	50.78	59.15	37.15	44.29	36.42
Number of Atoms						
Protein	4107	4048	3887	4060	4114	4165
Ligand	27	76	58	76	56	54
Water	151	100	125	244	264	156
Rmsd						
Bonds (Å)	0.012	0.011	0.009	0.011	0.010	0.010
Angles (°)	1.276	1.303	1.616	1.39	1.354	1.171
Ramachandran Analysis[5] (%)						
Core + Allowed	99.2	99.8	98.2	100	99.8	99.3
Generously allowed	0.9	0.2	1.8	0	0.2	0.6
Disallowed	0	0	0	0	0	0

[1] Values in parentheses correspond to the last shell.
[2] $R_{merge} = \Sigma |I - < I > | / \Sigma I$.
[3] $R_{free} = \Sigma |F_o - F_c| / \Sigma |F_o|$, for all data.
[4] $R_{work} = \Sigma |F_o - F_c| / \Sigma |F_o|$ for all data excluding data to used to calculate R_{free}.
[5] Calculated using PROCHECK.

was not observed for the intermediate agonist BVT.13 (Figure 6A). Contrary to previous models, these data suggest that weak activators of PPARγ (<80%) are not regulated through changes in stabilization or dynamics of H12. The β sheet region (amino acids 341–351) undergoes differential HDX following ligand binding (Figure 5), suggesting a possible role of this region of the LBD in ligand-mediated activation of the receptor. Full agonists afforded moderate stabilization, whereas MRL-24, nTZDpa, and BVT.13 induced robust protection from

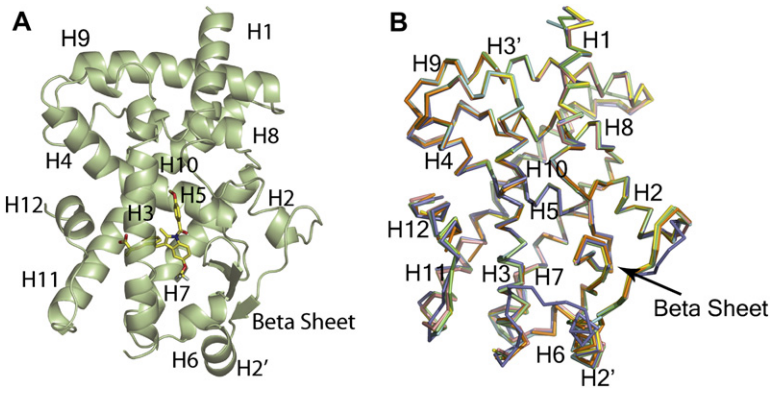

Figure 2. Overall Structure Comparison of PPARγ Bound to Agonists and Partial Agonists

(A) Ribbon diagram of PPARγ (green) bound to MRL-20 (yellow sticks).

(B) The figure shows a Cα trace of superimposed PPARγ monomers bound to rosiglitazone, MRL-20, MRL-24, nTZDpa, SR145, SR147, and BVT.13 Ligand-bound proteins colored as: rosiglitazone (PDB code: 2PRG) (Nolte et al., 1998) (purple), MRL-20 (forest green), MRL-24 (pink), nTZDpa (green), SR145 (cyan), SR147 (orange), and BVT.13 (yellow). Ligands are not shown.

exchange in this region. As discussed below, the crystal structures identified a common hydrogen bond network between these ligands, and the β sheet that was not found with the full agonists. Figure 6C suggests a compensatory mechanism of β sheet interaction to compensate for lack of H12 stabilization.

Among the six crystal structures, only the full agonist MRL-20 demonstrated the hydrogen bonding pattern to H12 that is observed in other full agonist crystal structures (Figures 7A and 7B), a feature consistent with the HDX data showing significant stabilization of H12. The partial agonists and intermediate agonist BVT.13 displayed no stabilization of H12, and no physical interaction with H12 was observed in the crystal structures as well (data not shown). With MRL-20, three hydrogen bonds extended from the acid of the lactate group to residues His323 (H6), His449 (H11), and Tyr473 (H12), as shown in Figure 7B. Hydrogen bonding with these residues has been seen in many agonist structures (Cronet et al., 2001; Ebdrup et al., 2003; Mahindroo et al., 2005; Nolte et al., 1998; Sauerberg et al., 2002) and is imperative for full activity of these compounds by direct stabilization of H12. Residue Ser289 formed a hydrogen bond with the ether oxygen of MRL-20 and was within hydrogen bonding distance of the acidic oxygen of the lactate group as well (Figure 7B), suggesting that this interaction may also indirectly contribute to the lactate interaction with H12.

Ligands That Do Not Robustly Stabilize H12 Stabilize the β sheet Region of the LBD

MRL-20 and MRL-24 showed an almost 180° rotation from each other within the ligand-binding pocket (Figure 7C), allowing for different atomic contacts that are reflected in unique changes to the dynamics of the LBD as determined by HDX analysis. In the partial agonist MRL-24 structure, the lactate group was found nestled against the β sheet making hydrogen bonds as well as hydrophobic and van der Waal contacts (Figure 7D). The acid portion of the lactate was positioned such that both oxygens are in hydrogen-bonding distance to contact the main chain amide nitrogen of Ser342 as well as a water-mediated contact to Glu343. The lactate group was positioned such that it was in contact distance with Ile341, Leu340, and Met348. This altered positioning of the lactate group, from ortho to meta, induced a flip in ligand positioning allowing interaction of the partial agonist MRL-24 with the β sheet. The observed binding mode of MRL-24 was consistent with the HDX data, which showed no statistically significant stabilization of H12 (Figure 5) but robust increased stabilization of the β sheet.

Both BVT.13 and nTZDpa also demonstrated stabilization of the β sheet relative to the full agonists as determined HDX. The indole of nTZDpa makes several contacts with the β sheet, mostly hydrophobic in nature, especially with Ile341 as shown in Figure 7E. The 2-carboxy group of the indole formed one direct hydrogen bond with Ser342 (2.76 Å) as well as a water-mediated hydrogen bond with Glu343. The position of the carboxylate of nTZDpa was rotated in perspective to that of BVT.13, only allowing one of the carboxylate oxygens to contact the β sheet directly.

In contrast to nTZDpa, the hydrogen bond network from BVT.13 to the β sheet was more extensive, differences that were reflected in the large protection in HDX (Figure 5). The carboxylate of BVT.13 had three contacts in hydrogen bonding distance to Ser342: two directly from each carboxylate oxygen (3.07 Å and 3.35 Å) as well as a water-mediated bond (Figure 7F). These changes in atomic contacts were reflected in the HDX kinetics for residues 341–351, with a 29% reduction in rate for nTZDpa as compared to a 37% reduction for BVT.13, differences that were statistically significant ($p < 0.001$). In addition, the benzoyl group of BVT.13 contained two chlorines, whereas, the benzyl group in nTZDpa contained only one. One of the chlorines of BVT.13 was positioned to make a tighter van der Waal surface with the β sheet (residue Leu340) as seen in Figure 7F. This space filling was not available in the nTZDpa structure to contact the β sheet, as the benzyl group only consists of one chlorine which was positioned further away at the H3 and H5 interface. Thus, these data demonstrate that HDX can discriminate subtle atomic differences in the interaction of ligands with receptor.

The combination of HDX and crystallography has identified the hydrogen bonding between ligand and β sheet as an epitope for high-affinity interaction with partial agonists. It is notable that previously described partial agonist crystal structures including that of GW0072

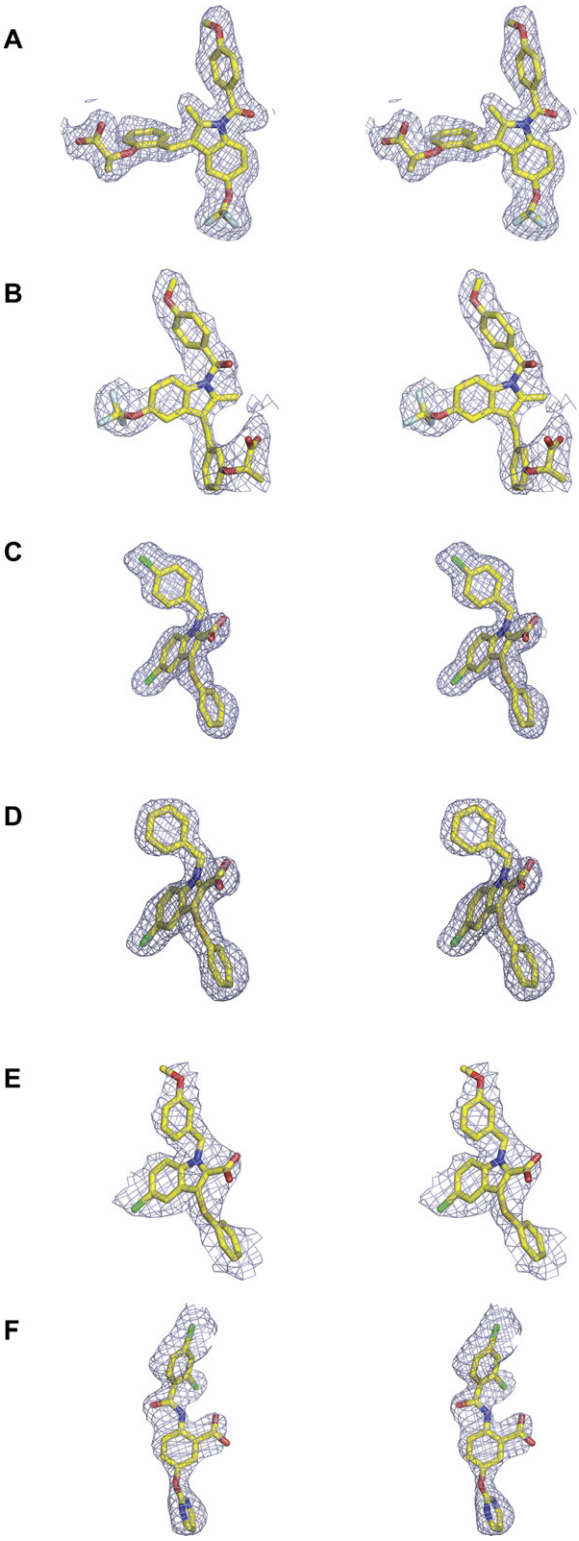

Figure 3. Stereo View of Electron Density

Electron density is shown from composite omit $2F_o$-F_c maps (contoured at 1σ) of ligands, with the exception of SR147, which was calculated as an omit map with ligand model deleted.

(A) MRL-20.
(B) MRL-24.
(C) nTZDpa.
(D) SR145.
(E) SR147.
(F) BVT.13.

demonstrate a hydrogen bond between ligand and the β sheet, highlighting the importance of this structural feature (Oberfield et al., 1999). Thus, targeting the β sheet for high-affinity interaction with the receptor, rather than H12, defines a broadly used binding epitope for partial agonists.

H3 Is Differentially Stabilized as a Function of Binding Mode

Among the full and partial agonists tested, ligands were broadly grouped into those that occupy the portion of the LBD spanning from H11 and H12 beyond H3 (rosiglitazone, MRL-20, and MRL-24) and those that occupy the region between H3 and the β sheet only (nTZDpa and BVT.13). The previously described GW0072 ligand would fall into the second class. Among both classes of compounds, the partial agonists showed differential stabilization of H3 when compared to the full agonists. With the first class of compounds, stronger transactivation was achieved with a corresponding decrease in stabilization of H3 (Figure 6D); this can perhaps be explained by the ability of the compounds in this area to achieve increases in transactivation by directly stabilizing H12. In contrast, compounds unable to directly contact H12 showed increased stabilization of H3 in proportion with transactivation efficacy (Figure 6E).

The HDX studies revealed increased stabilization of H3 with the partial agonist MRL-24 (46%) relative to MRL-20 (34%), differences that are significant (p value < 0.0001) and consistent with the differences in ligand-binding modes. MRL-20 was positioned closer to H3 than MRL-24 and was in contact distance with Ile281, Gly284, Cys285, Arg288, and Ala292 (Figure 8A). Due to its size and proximity, the ring bearing the lactate group of MRL-24 formed closer and more numerous hydrophobic contacts and van der Waals contacts with residues Cys285, Gly284, and Ile281. Although the trifluoromethoxy group of MRL-20 inserted close to H3 in the same region, it did not extend across as large an area or as closely as MRL-24, possibly due to the dispersive nature of the fluorines. In addition, the Arg288 side chain was pulled closer to the MRL-24 ligand than the MRL-20 ligand, making two hydrogen bonds with MRL-24. Neither full agonist ligand MRL-20 nor rosiglitazone made hydrogen-bonding patterns with Arg288. Thus, the differences in HDX kinetics for H3 reflected subtle structural differences in ligand interaction with the receptor, highlighting the relative strengths of these approaches to identify critical regions of stabilization and explain the molecular details, respectively.

Differences in HDX kinetics between BVT.13 and nTZDpa can be explained by BVT.13 contacting a larger

Sequence	Residues Start	End	z	2° Structure[1]	Rosi	BVT.13	MRL-20	MRL-24	nTZDpa
RALAKHLYDSY	212	222	2	H 1	0%	−2%	−12%	−13%	−9%
IRIFQGCQF	279	287	2	H 3	−22%	−46%	−34%	−46%	−34%
YAKSIPGFVNL	299	309	2	3–4 Loop	1%	−1%	−15%	−15%	−10%
LKYGVHEIIY	318	327	2	H 5	−6%	−2%	−10%	−7%	−6%
LKYGVHE	318	324	2	H 5	−10%	−4%	−14%	−12%	−7%
ASLMNKDGVL	331	340	1	B 2–3	−15%	−20%	−26%	−27%	−20%
ISEGQGFMTRE	341	351	2	B 4	−12%	−37%	−19%	−28%	−29%
FLKSLRKPFGDFMEPKFEF	352	370	3	H 6–7	−8%	−14%	−17%	−20%	−14%
FLKSLRKPFGDF	352	363	3	H 6–7	−3%	−14%	−11%	−16%	−11%
MEPKFEF	364	370	2	H 7	−15%	−17%	−24%	−24%	−21%
AVKFNALE	371	378	2	H 7	−11%	−6%	−18%	−17%	−13%
AVKFNAL	371	377	2	H 7	−9%	−7%	−20%	−19%	−16%
VIILSGDRPGLL	390	401	2	H 8–9	−2%	−1%	−10%	−9%	−5%
IILSGDRPGLL	391	401	2	H 8	−2%	−1%	−10%	−9%	−5%
NVKPIED	402	408	1	H 9	0%	−1%	−10%	−11%	−6%
LQLKLNHPESSQL	419	431	2	H 9–10	0%	−2%	−7%	−8%	−3%
QLKLNHPESSQL	420	431	2	H 9–10	1%	0%	−4%	−8%	−4%
LKLNHPESSQL	421	431	2	H 9–10	2%	0%	0%	−4%	−2%
KLNHPESSQL	422	431	2	H 9–10	1%	0%	2%	−2%	0%
FAKLLQKMTDL	432	442	2	H 10–11	−1%	−5%	−16%	−12%	−9%
FAKLLQKMTDL	432	442	3	H 10–11	−1%	−5%	−16%	−9%	−9%
RQIVTEHVQL	443	452	2	H 10–11	−26%	−6%	−25%	−10%	−5%
RQIVTE	443	448	2	H 10–11	−23%	−5%	−22%	−5%	−7%
IVTEHVQL	445	452	2	H 10–11	−21%	1%	−20%	−7%	−2%
LQVIKKTETDMSLHPLL	453	469	3	H 11–12	−6%	−4%	−6%	−5%	0%
LQVIKKTETDMSLHPLL	453	469	2	H 11–12	−4%	−3%	−6%	−6%	0%
LQVIKKTETDMSLHPLLQEIYKDLY	453	477	3	H 11–12	−9%	−1%	−5%	−3%	2%
LQVIKKTETDMSLHPLLQEIYKDLY	453	477	4	H 11–12	−9%	−1%	−5%	−3%	2%
SLHPLLQEIYKDLY	464	477	2	H 11–12	−14%	1%	−7%	1%	2%
QEIYKDLY	470	477	1	H 12	−13%	2%	−7%	−2%	−1%
QEIYKDLY	470	477	2	H 12	−16%	0%	−8%	1%	1%

[1]Secondary structure regions as described in Uppenberg et al., 1998.

H, Helix; B, β sheet.

Figure 4. Changes in H/D Exchange Rates for Regions of PPARγ LBD upon Binding of Ligands
Secondary structure regions as described in Uppenberg et al., 1998.

surface area of H3 than nTZDpa, making different hydrogen bonds with H3, as well as making more hydrophobic contacts overall. Both structures made several contacts with Arg288 found on H3. In the nTZDpa structure, Arg288, as with other full and partial agonists, extended across a large portion of the ligand, clamping it in place between H3 and the β sheet. In contrast, BVT.13 was positioned closer to Arg288 than nTZDpa, allowing for more hydrophobic and van der Waals contacts (Figures 7E and 7F). There were also differences between nTZDpa and BVT.13 in the manner of interaction with a large portion of H3. The thiophenyl group of nTZDpa extended parallel along H3 and made hydrophobic contacts with Ile247, Leu255, Glu259, Met348, and Ile281. On the other hand, BVT.13 extended deeper into the region between the lower portion of H3 and H2′ (Figure 8B). The pyrimidine ring of BVT.13 afforded a hydrogen bond contact with His266 (3.42 Å), but this interaction was absent in the nTZDpa structure. There was also a stacking interaction with the pyrimidine ring and Phe264 that was not observed in the nTZDpa structure. These structural observations suggested that the increased protection in H/D exchange in this region directly reflected ligand-mediated stabilization of the secondary structural elements.

DISCUSSION

Graded transcriptional responses have been suggested to derive from differential modulation of H12 (Kallenberger et al., 2003; Nagy and Schwabe, 2004; Nettles and Greene, 2005). In the work presented here, we employed quantitative amide HDX to demonstrate that only full agonists stabilize H12. Ligands that afford weak or intermediate levels of transactivation (<80% TA) are not associated with statistically significant stabilization of H12. We also show that stabilization of H3 and H11 are not sufficient to stabilize H12, suggesting that coactivator recruitment by partial agonists derives from a distinct mechanism (Burgermeister et al., 2006; Fujimura et al., 2006).

What is the mechanism of high-affinity ligands affording varying magnitudes of agonism of PPARγ? It is clear that partial agonists stabilize the LBD in a distinct manner in comparison to full agonists. Previous studies using NMR have shown that full agonists stabilize large portions of the LBD (Berger et al., 2003; Johnson et al., 2000; Klein et al., 2005). Fluorescence anisotropy was employed to demonstrate full-agonist stabilization of H12 (Kallenberger et al., 2003). Our studies showed that compounds that do not stabilize H12 differentially stabilize other regions of the LBD, and the magnitude of transactivation varied

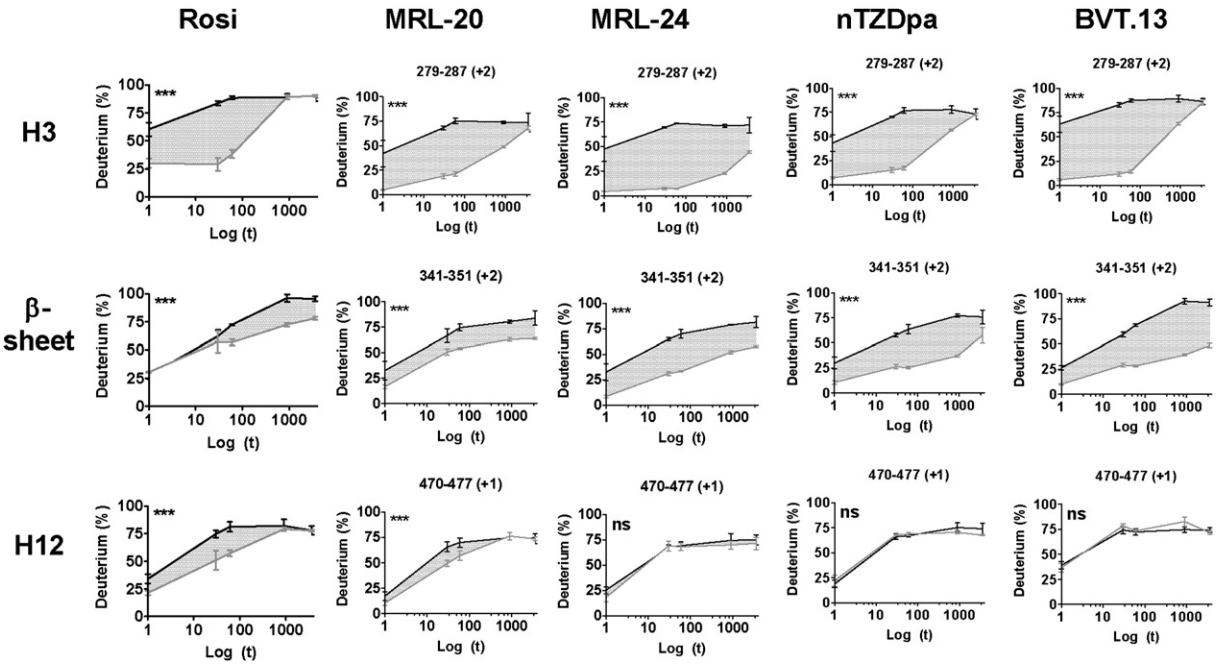

Figure 5. Differential H/D Exchange Data Plotted as a Percentage Incorporation of Deuterium versus Time in Seconds

HDX data for the apo PPARγ LBD is represented by the black line. The gray line represents the HDX data for the ligand-bound PPARγ LBD. The shaded region between the lines represents the percentage reduction in HDX values that make up the data in Figure 4. All ligands induced a reduction of exchange rate for H3 (residues 279–287) upon binding. MRL-20 and nTZDpa reduced exchange rate to a lesser degree than MRL-24 and BVT.13. The β sheet region (341–351) showed a gradient in reduction of exchange rate upon binding MRL-20, MRL-24, nTZDpa, and BVT.13. Only the full agonists rosiglitazone and MRL-20 stabilized H12 (residues 470–477) to a statistically significant extent providing direct evidence that stabilization of H12 is not required for activation of PPARγ. Statistical summary from a 2-way ANOVA between apo and ligand bound data: ***, $p < 0.001$; **, $p < 0.001$–0.01; *, $p < 0.01$–0.5; ns, not significant. The value in parenthesis represents the charge state of the peptide ion. Error bars represent the standard deviation around the mean value where n = 4.

depending on the overall stabilization pattern induced by the ligand. For example, BVT.13 preferentially stabilized the β sheet and H3 to a larger degree than nTZDpa, while the partial agonist MRL-24 preferentially stabilized the β sheet and H3 to a larger degree than MRL-20. Since there was no change in conformation upon binding these various ligands, full agonists may function by directly stabilizing the AF-2 coactivator binding site, while partial agonists only stabilize regions away from H12, leaving H12 in a highly dynamic state. This differential stabilization may also transmit to regions of the receptor away from AF-2, such as the β sheet, suggesting a distinct coactivator-binding surface, consistent with the findings that regions outside the LxxLL motifs contribute to receptor binding (Klein et al., 2005; Puigserver et al., 1998). Another possibility is that non-AF-2 coactivator recruitment could be facilitated by conformational changes induced in the dimer partner, RXR, which could not be tested here. However, further improvements in our HDX platform are underway to facilitate analysis of dynamics of the PPAR/RXR heterodimer as a function of ligand. The results presented here highlight that understanding allosteric communication between ligand- and coactivator-binding sites requires analysis of both high-resolution structure and conformational dynamics.

In summary, we have shown through X-ray crystallography and HDX that subtle differences among PPARγ ligands can elicit statistically significant differences in receptor dynamics, binding mode, and degree of agonist activity. Here we demonstrate that agonists with less than 80% transactivation efficacy as compared to rosiglitazone do not stabilize H12, suggesting that a non-H12-dependent mechanism exists to control coactivator recruitment to the receptor in response to this class of ligand. Among the ligands lacking full agonist activity, all demonstrated protection from exchange in the β sheet region, allowing high-affinity ligand interaction with PPARγ. An analysis of paired ligands further demonstrates that subtle atomic differences in ligand-binding modes were reflected in the HDX analysis, highlighting the strength of this approach to rapidly and sensitively probe ligand-binding mode and structural dynamics.

EXPERIMENTAL PROCEDURES

Cell-Based Transactivation Assay

COS-1 cells were seeded at 12×10^3 cells/well in 96-well cell culture plates in high-glucose Dulbecco's modified Eagle's medium containing 10% fetal bovine serum (Hyclone), nonessential amino acids, 100 units/ml penicillin G, and 100 mg/ml streptomycin sulfate at 37°C in

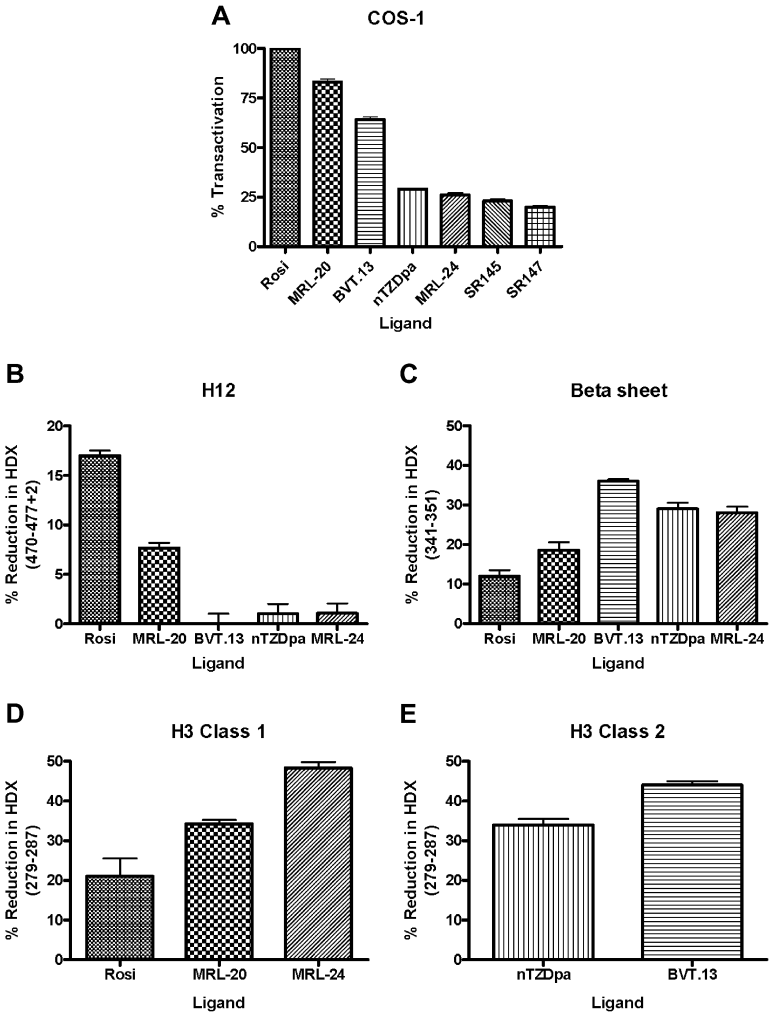

Figure 6. Comparison of HDX Data among Different Ligands within the Helix 12, Helix 3, and β Sheet Regions

(A) Cell-based transactivation data.

(B) Helix 12 is only stabilized by full agonists. Partial and intermediate agonists show no statistically significant stabilization pattern compared to the apo structure.

(C) Partial agonists preferentially stabilize the β sheet.

(D) Class I ligands with weaker transaction profiles preferentially stabilize helix 3.

(E) Class II ligands with stronger transactivation profiles preferentially stabilize helix 3.

Error bars represent the standard deviation around the mean value where n = 3 (A) and n = 4 (B–E).

a humidified atmosphere of 5% CO_2. After 24 h, transfections were performed with LipofectAMINE (Life Technologies Inc.) according to the instructions of the manufacturer. Briefly, transfection mixes for each well contained 0.25 mg of each expression vector containing full-length PPARγ, peroxisome proliferator-activated receptor response element (PPRE), DR1-Luciferase reporter, and LipofectAMINE reagent at a ratio of 1:5 (mg of DNA/ml of reagent). Cells were incubated in the transfection mixture for 6 hr at 37°C in a humidified atmosphere of 5% CO_2. The cells were then washed with phosphate-buffered saline and incubated for ~24 hr in fresh high-glucose Dulbecco's modified Eagle's medium containing 5% fetal calf serum, nonessential amino acids, 100 units/ml penicillin G, and 100 mg/ml streptomycin sulfate ± increasing concentrations of test compound. Since the compounds were solubilized in DMSO, control cells were incubated with equivalent concentrations of DMSO; final DMSO concentrations were equal to 0.1%, a concentration that was shown not to affect transactivation activity. Cells were harvested and lysates were produced using reporter lysis buffer (Promega) according to the manufacturer's instructions. Luciferase activity in cell extracts was determined using Luciferase assay buffer (Promega) in a luminometer (Analyst GT, Molecular Devices).

Biochemical Coactivator Recruitment Assay Using FRET

Sample wells contain a mixture of 1 nM GST-PPARγLBD, 2 nM anti-GST-(Eu)K, 10 nM FLAG-SRC1, 20 nM anti-FLAGXL665, and 2 μl test compound in buffer containing 100 mM phosphate, 125 mM KF, 0.5% (wt/vol) 3-[(3-cholamidopropyl) dimethyl-ammonio]-1-propanesulfonate (CHAPS), 0.1% BSA, in a volume of 100 μl (96-well format). These reactions were routinely incubated overnight at 4°C. The mixtures are irradiated at 330 nm (corresponding to the europium absorption band) and the fluorescence emission intensity of the XL665 acceptor at 620 nm and 665 nm are simultaneously recorded with 50 μs time delay and an integration time of 0.2 s. Data were typically expressed as the ratio, multiplied by a factor of 10^4, of the fluorescence intensity at 665 nm to that at 620 nm. Agonist dose-response was generated by titrating increasing concentrations of compound and measuring FRET after each addition.

PPARγ Protein Expression and Purification

DNA encoding the LBD of PPARγ (encoding amino acids 205–477) was amplified by PCR and cloned into the expression vector pMCSG19 (Stols et al., 2002). This expression construct produced an N-terminal MBP (maltose binding protein) fused to PPARγ with a TEV (tobacco etch virus) protease recognition site for removal of MBP. The plasmid pMCSG13-PPARγ-LBD was transformed into *E. coli* Rosetta cells (Novagen). Cells were grown at 37°C in LB medium containing 30 μg/ml chloramphenicol and 50 μg/ml ampicillin. Expression of PPARγ was induced by the addition of isopropyl β-D-thiogalactoside to a final concentration of 0.5 mM and grown an additional 16–18 hr. Cells were resuspended in 20 mM Tris-HCl (pH 8.0), 0.5 M NaCl,

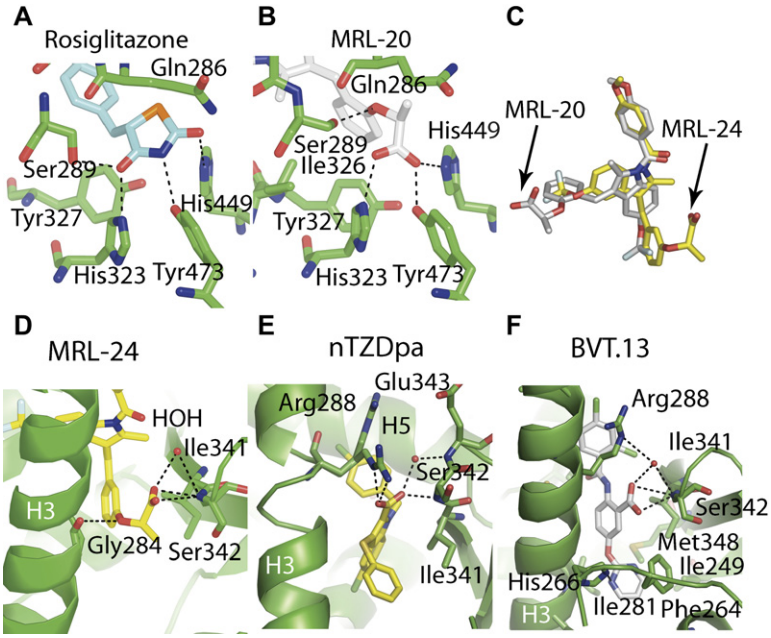

Figure 7. Structural Details of Hydrogen-Bonding Networks of Full and Partial Agonists

PPARγ (green), rosiglitazone (blue), MRL-20 (white), MRL-24 (yellow), nTZDpa (yellow), and BVT.13 (white).

(A) Hydrogen-bonding network of the rosiglitazone (PDB code: 2PRG) TZD head group to conserved PPARγ residues (Nolte et al., 1998).

(B) Hydrogen-bonding network of the MRL-20 lactate group to conserved PPARγ residues.

(C) MRL-20 and MRL-24 represented as stick figures as they lie in the binding pocket generated by superimposition of the respective protein molecules.

(D) The lactate group of MRL-24 contacts the β sheet making several hydrogen bonds.

(E) The hydrogen bonding network of nTZDpa contacts the β sheet and Arg288 adopts two defined conformations.

(F) The hydrogen bonding network of BVT.13 contacts the β sheet.

10mM imidazole, 10% glycerol, and 5 mM BME (β-mercaptoethanol). 20 mM Tris (pH 8.0), 5 mM BME, and 10% glycerol were included in all buffers following lysis. Cells were lysed by sonication and pelleted by centrifugation. The supernatant was applied to a 5 ml His-Trap FF crude column (GE Healthcare). PPARγ was eluted with an imidazole gradient (0.01–0.5 M). Fractions containing PPARγ were pooled and dialyzed to 2 liters dialysis buffer containing 1 mM imidazole and 20 mM NaCl. In addition, the MBP fusion was removed proteolytically using TEV protease at a weight ratio of 20:1 (fusion protein:TEV protease) during dialysis. To remove TEV protease, MBP, and nonproteolyzed MBP-PPARγ, the dialyzed protein solution was passed over a 5 ml His-Trap FF crude column (GE Healthcare) again and the flow-through was collected. PPARγ was then applied to a Mono Q HR 10/10 column (GE Healthcare) and eluted with a linear NaCl gradient (0.01–0.5 M). PPARγ was dialyzed extensively to 20 mM Tris-HCl (pH 8.0), 10% glycerol, 150 mM NaCl, and 1 mM DTT. PPARγ was concentrated to 10 mg/ml using a 10,000 molecular weight cut off Amicon Ultra 15 centrifugal concentrator (Millapore) and flash frozen prior to storage at −130°C. Finally, the purity of the protein was confirmed by ESI MS. A single component corresponding to the mass of the PPARγ LBD was identified (data not shown).

Crystallization and Data Collection

Crystals of apo-PPARγ were grown by vapor diffusion in hanging drops at 20°C. PPARγ (1 μl) was mixed with 1 μl well solution containing 1.3 M sodium citrate (pH 5.6) and 20 mM Tris-HCL (pH 8.0). Cubic-shaped crystals grew within 3–7 days. PPARγ ligands were soaked into PPARγ apo-crystals by adding 0.5 μl of compound at a concentration of 5 mM suspended in well solution containing 5% DMSO (not all compounds were soluble at this concentration; solution containing precipitated compound was added to crystal drops when necessary) directly to the crystal drop. Crystals were soaked from 3 days to 3 weeks depending on the compound. All crystals were transferred to a cryoprotectant comprised of well solution containing 20% glycerol and covered with paraffin oil, and flash frozen. The measurements were carried out using 10 s exposures at the synchrotron and 360° (using 1° increments) of crystal data were collected. This amounted to approximately 2–4 hr of data collection

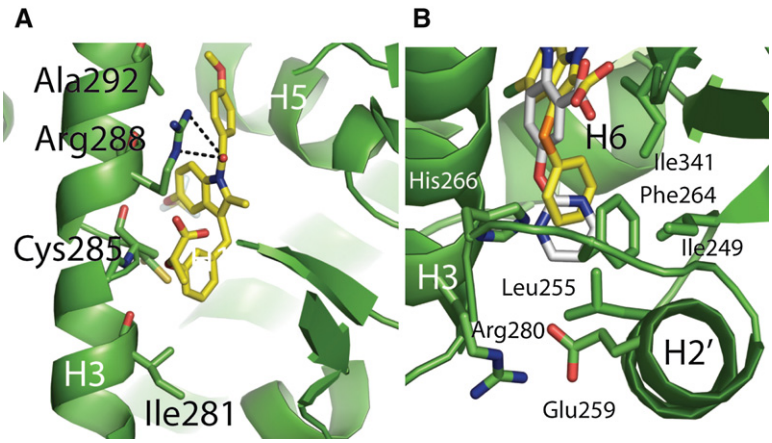

Figure 8. Structural Details of H3 and H2′ Ligand Packing with PPARγ Shown in Green

(A) Partial agonist MRL-24 (yellow) lies close to H3 and makes more contacts to H3 than its full agonist counterpart MRL-20.

(B) Superimposition of the nTZDpa ligand (yellow) onto the BVT.13 (white) structure highlighting contacts of the lower portion of H3, H2′ and the adjoining loop.

time. There was no observed radiation decay of the crystals over the course of data collection as monitored by comparing the intensities and the resolution of reflections of the initial frames to the final frames.

Structure Determination and Refinement

Data was collected at the APS SER-CAT and SSRL BL1-11 beamlines and processed with HKL2000 (Otwinowski and Minor, 1997). All structures were solved by molecular replacement using MOLREP in CCP4 (CCP4, 1994) and the previously published PPARγ structure (PDB code: 1KNU) (Sauerberg et al., 2002) as the search model. To avoid biasing our maps, all water molecules and ligands were excluded. Refinement of all structures was carried out in CCP4 (CCP4, 1994) and model building was carried out in Coot (Emsley and Cowtan, 2004). Difference Fourier maps gave strong and clear density to build all ligands. Several rounds of manual rebuilding in Coot followed by refinement in CCP4 were carried out. TLS refinement was carried out with most of the structures.

HDX Analysis

Solution-phase amide HDX was performed with a fully automated system that is described in detail elsewhere (Chalmers et al., 2006). Briefly, 4 μl of a 10 μM protein solution (20 mM Tris-CL [pH 7.9], containing 20% glycerol, 100 mM KCl, 0.2 M EDTA, 1 mM DTT) was diluted to 20 μl with D2O dilution buffer (20 mM Tris-CL [pH 7.9], containing 100 mM KCl, 1 mM DTT) and incubated at 25°C for the following periods of time: 1, 30, 60, 900, and 3600 s. Each differential HDX experiment required approximately 2 nmol of total protein. Following on-exchange, unwanted forward or back exchange was minimized and the protein was denatured by dilution to 50 μl with 0.1% TFA in 2 M urea (held at 1°C). Sample was then passed across an immobilized pepsin column (prepared in house) at 200 μl min-1 (0.1% TFA, 1°C) and the resulting peptides were trapped onto a C_{18} trap cartridge (Microm Bioresources). Peptides were then gradient eluted (4% CH_3CN to 40% CH_3CN, 0.3% formic acid over 15 min, 2°C) across a 2.1 mm × 50 mm C_{18} HPLC column (Hypersil Gold, Thermo Electron) and electrosprayed directly into a linear ion trap mass spectrometer (LTQ, Thermo Electron). Data were processed with in-house software (Pascal et al., 2007) and Microsoft Excel and visualized with pyMOL (DeLano Scientific). To measure the difference in exchange rates, we calculated the average percentage deuterium uptake for 27 regions of the apo PPARγ LBD following 1, 30, 60, 900, and 3600 s of on-exchange. From this value, we subtract the average percent deuterium uptake measured for the PPARγ LBD + ligand complex.

Chemical Synthesis of Ligands

The PPARγ agonists MRL-20, MRL-24, nTZDpa, SR147, and SR145 were synthesized following previously described chemical strategies (Acton et al., 2005; Berger et al., 2003) and were isolated to >98% purity. Rosiglitazone was purchased from ChemPacific Corp.

Supplemental Data

Supplemental data including one supplemental figure are available online at http://www.structure.org/cgi/content/full/15/10/1258/DC1/.

ACKNOWLEDGMENTS

The authors thank B. Pascal and M. Southern for software engineering support. The authors also wish to thank J. Chrzas, G. Sahle, and J. Habel for data collection at APS SER-CAT and C. Smith, G. Card, and J. Habel for data collection at SSRL beamlines. Portions of data were collected at Southeast Regional Collaborative Access Team (SER-CAT) 22-ID (or 22-BM) beamline at the Advanced Photon Source, Argonne National Laboratory. Portions of this research were carried out at the Stanford Synchrotron Radiation Laboratory, a national user facility operated by Stanford University on behalf of the U.S. Department of Energy, Office of Basic Energy Sciences. The Scripps Research Institute is supported by the State of Florida. Crystallography questions should be addressed to Dr. Nettles and HDX questions should be addressed to Dr. Griffin.

Received: June 12, 2007
Revised: July 25, 2007
Accepted: July 31, 2007
Published: October 16, 2007

REFERENCES

Acton, J.J., 3rd, Black, R.M., Jones, A.B., Moller, D.E., Colwell, L., Doebber, T.W., Macnaul, K.L., Berger, J., and Wood, H.B. (2005). Benzoyl 2-methyl indoles as selective PPARgamma modulators. Bioorg. Med. Chem. Lett. *15*, 357–362.

Bendixen, A.C., Shevde, N.K., Dienger, K.M., Willson, T.M., Funk, C.D., and Pike, J.W. (2001). IL-4 inhibits osteoclast formation through a direct action on osteoclast precursors via peroxisome proliferator-activated receptor gamma 1. Proc. Natl. Acad. Sci. USA *98*, 2443–2448.

Berger, J., and Wagner, J.A. (2002). Physiological and therapeutic roles of peroxisome proliferator-activated receptors. Diabetes Technol. Ther. *4*, 163–174.

Berger, J.P., Petro, A.E., Macnaul, K.L., Kelly, L.J., Zhang, B.B., Richards, K., Elbrecht, A., Johnson, B.A., Zhou, G., Doebber, T.W., et al. (2003). Distinct properties and advantages of a novel peroxisome proliferator-activated protein [gamma] selective modulator. Mol. Endocrinol. *17*, 662–676.

Berger, J.P., Akiyama, T.E., and Meinke, P.T. (2005). PPARs: therapeutic targets for metabolic disease. Trends Pharmacol. Sci. *26*, 244–251.

Burgermeister, E., Schnoebelen, A., Flament, A., Benz, J., Stihle, M., Gsell, B., Rufer, A., Ruf, A., Kuhn, B., Marki, H.P., et al. (2006). A novel partial agonist of peroxisome proliferator-activated receptor-gamma (PPARgamma) recruits PPARgamma-coactivator-1alpha, prevents triglyceride accumulation, and potentiates insulin signaling in vitro. Mol. Endocrinol. *20*, 809–830.

CCP4. (1994). The CCP4 suite: programs for protein crystallography. Acta Crystallogr. D Biol. Crystallogr. *50*, 760–763.

Chalmers, M.J., Busby, S.A., Pascal, B.D., He, Y., Hendrickson, C.L., Marshall, A.G., and Griffin, P.R. (2006). Probing protein ligand interactions by automated hydrogen/deuterium exchange mass spectrometry. Anal. Chem. *78*, 1005–1014.

Chawla, A., Repa, J.J., Evans, R.M., and Mangelsdorf, D.J. (2001). Nuclear receptors and lipid physiology: opening the X-files. Science *294*, 1866–1870.

Cronet, P., Petersen, J.F., Folmer, R., Blomberg, N., Sjoblom, K., Karlsson, U., Lindstedt, E.L., and Bamberg, K. (2001). Structure of the PPARalpha and -gamma ligand binding domain in complex with AZ 242; ligand selectivity and agonist activation in the PPAR family. Structure *9*, 699–706.

Day, C. (1999). Thiazolidinediones: a new class of antidiabetic drugs. Diabet. Med. *16*, 179–192.

Ebdrup, S., Pettersson, I., Rasmussen, H.B., Deussen, H.J., Frost Jensen, A., Mortensen, S.B., Fleckner, J., Pridal, L., Nygaard, L., and Sauerberg, P. (2003). Synthesis and biological and structural characterization of the dual-acting peroxisome proliferator-activated receptor alpha/gamma agonist ragaglitazar. J. Med. Chem. *46*, 1306–1317.

Elbrecht, A., Chen, Y., Adams, A., Berger, J., Griffin, P., Klatt, T., Zhang, B., Menke, J., Zhou, G., Smith, R.G., and Moller, D.E. (1999). L-764406 is a partial agonist of human peroxisome proliferator-activated receptor gamma. The role of Cys313 in ligand binding. J. Biol. Chem. *274*, 7913–7922.

Emsley, P., and Cowtan, K. (2004). Coot: model-building tools for molecular graphics. Acta Crystallogr. D Biol. Crystallogr. *60*, 2126–2132.

Englander, S.W. (2006). Hydrogen exchange and mass spectrometry: a historical perspective. J. Am. Soc. Mass. Spectrom. *17*, 1481–1489.

Forman, B.M., Tontonoz, P., Chen, J., Brun, R.P., Spiegelman, B.M., and Evans, R.M. (1995). 15-Deoxy-delta 12, 14-prostaglandin J2 is a ligand for the adipocyte determination factor PPAR gamma. Cell *83*, 803–812.

Fujimura, T., Sakuma, H., Konishi, S., Oe, T., Hosogai, N., Kimura, C., Aramori, I., and Mutoh, S. (2005). FK614, a novel peroxisome proliferator-activated receptor gamma modulator, induces differential transactivation through a unique ligand-specific interaction with transcriptional coactivators. J. Pharmacol. Sci. *99*, 342–352.

Fujimura, T., Sakuma, H., Ohkubo-Suzuki, A., Aramori, I., and Mutoh, S. (2006). Unique properties of coactivator recruitment caused by differential binding of FK614, an anti-diabetic agent, to peroxisome proliferator-activated receptor gamma. Biol. Pharm. Bull. *29*, 423–429.

Gottlicher, M., Widmark, E., Li, Q., and Gustafsson, J.A. (1992). Fatty acids activate a chimera of the clofibric acid-activated receptor and the glucocorticoid receptor. Proc. Natl. Acad. Sci. USA *89*, 4653–4657.

Greene, D.A. (1999). Rosiglitazone: a new therapy for Type 2 diabetes. Expert Opin. Investig. Drugs *8*, 1709–1719.

Hamuro, Y., Coales, S.J., Morrow, J.A., Molnar, K.S., Tuske, S.J., Southern, M.R., and Griffin, P.R. (2006). Hydrogen/deuterium-exchange (H/D-Ex) of PPARgamma LBD in the presence of various modulators. Protein Sci. *15*, 1883–1892.

Johnson, B.A., Wilson, E.M., Li, Y., Moller, D.E., Smith, R.G., and Zhou, G. (2000). Ligand-induced stabilization of PPARgamma monitored by NMR spectroscopy: implications for nuclear receptor activation. J. Mol. Biol. *298*, 187–194.

Kallenberger, B.C., Love, J.D., Chatterjee, V.K., and Schwabe, J.W. (2003). A dynamic mechanism of nuclear receptor activation and its perturbation in a human disease. Nat. Struct. Biol. *10*, 136–140.

Klein, F.A., Atkinson, R.A., Potier, N., Moras, D., and Cavarelli, J. (2005). Biochemical and NMR mapping of the interface between CREB-binding protein and ligand binding domains of nuclear receptor: beyond the LXXLL motif. J. Biol. Chem. *280*, 5682–5692.

Kliewer, S.A., Umesono, K., Noonan, D.J., Heyman, R.A., and Evans, R.M. (1992). Convergence of 9-cis retinoic acid and peroxisome proliferator signalling pathways through heterodimer formation of their receptors. Nature *358*, 771–774.

Kliewer, S.A., Sundseth, S.S., Jones, S.A., Brown, P.J., Wisely, G.B., Koble, C.S., Devchand, P., Wahli, W., Willson, T.M., Lenhard, J.M., and Lehmann, J.M. (1997). Fatty acids and eicosanoids regulate gene expression through direct interactions with peroxisome proliferator-activated receptors alpha and gamma. Proc. Natl. Acad. Sci. USA *94*, 4318–4323.

Mahindroo, N., Huang, C.F., Peng, Y.H., Wang, C.C., Liao, C.C., Lien, T.W., Chittimalla, S.K., Huang, W.J., Chai, C.H., Prakash, E., et al. (2005). Novel indole-based peroxisome proliferator-activated receptor agonists: design, SAR, structural biology, and biological activities. J. Med. Chem. *48*, 8194–8208.

Maier, C.S., and Deinzer, M.L. (2005). Protein conformations, interactions, and H/D exchange. Methods Enzymol. *402*, 312–360.

Nagy, L., and Schwabe, J.W. (2004). Mechanism of the nuclear receptor molecular switch. Trends Biochem. Sci. *29*, 317–324.

Nagy, L., Kao, H.Y., Love, J.D., Li, C., Banayo, E., Gooch, J.T., Krishna, V., Chatterjee, K., Evans, R.M., and Schwabe, J.W. (1999). Mechanism of corepressor binding and release from nuclear hormone receptors. Genes Dev. *13*, 3209–3216.

Nettles, K.W., and Greene, G.L. (2005). Ligand control of coregulator recruitment to nuclear receptors. Annu. Rev. Physiol. *67*, 309–333.

Nissen, S.E., and Wolski, K. (2007). Effect of rosiglitazone on the risk of myocardial infarction and death from cardiovascular causes. N. Engl. J. Med. *356*, 2457–2471.

Nolte, R.T., Wisely, G.B., Westin, S., Cobb, J.E., Lambert, M.H., Kurokawa, R., Rosenfeld, M.G., Willson, T.M., Glass, C.K., and Milburn, M.V. (1998). Ligand binding and co-activator assembly of the peroxisome proliferator-activated receptor-gamma. Nature *395*, 137–143.

Oberfield, J.L., Collins, J.L., Holmes, C.P., Goreham, D.M., Cooper, J.P., Cobb, J.E., Lenhard, J.M., Hull-Ryde, E.A., Mohr, C.P., Blanchard, S.G., et al. (1999). A peroxisome proliferator-activated receptor gamma ligand inhibits adipocyte differentiation. Proc. Natl. Acad. Sci. USA *96*, 6102–6106.

Ostberg, T., Svensson, S., Selen, G., Uppenberg, J., Thor, M., Sundbom, M., Sydow-Backman, M., Gustavsson, A.L., and Jendeberg, L. (2004). A new class of peroxisome proliferator-activated receptor agonists with a novel binding epitope shows antidiabetic effects. J. Biol. Chem. *279*, 41124–41130.

Otwinowski, Z., and Minor, A. (1997). Processing of X-ray diffraction data collected in oscillation mode. Methods Enzymol. *276*, 307–326.

Pascal, B.D., Chalmers, M.J., Busby, S.A., Mader, C.C., Southern, M.R., Tsinoremas, N.F., and Griffin, P.R. (2007). The Deuterator: software for the determination of backbone amide deuterium levels from H/D exchange MS data. BMC Bioinformatics *8*, 156.

Pearson, S.L., Cawthorne, M.A., Clapham, J.C., Dunmore, S.J., Holmes, S.D., Moore, G.B., Smith, S.A., and Tadayyon, M. (1996). The thiazolidinedione insulin sensitiser, BRL 49653, increases the expression of PPAR-gamma and aP2 in adipose tissue of high-fat-fed rats. Biochem. Biophys. Res. Commun. *229*, 752–757.

Puigserver, P., Wu, Z., Park, C.W., Graves, R., Wright, M., and Spiegelman, B.M. (1998). A cold-inducible coactivator of nuclear receptors linked to adaptive thermogenesis. Cell *92*, 829–839.

Rangwala, S.M., and Lazar, M.A. (2002). The dawn of the SPPARMs? Sci. STKE *2002*, PE9.

Rocchi, S., Picard, F., Vamecq, J., Gelman, L., Potier, N., Zeyer, D., Dubuquoy, L., Bac, P., Champy, M.F., Plunket, K.D., et al. (2001). A unique PPARgamma ligand with potent insulin-sensitizing yet weak adipogenic activity. Mol. Cell *8*, 737–747.

Rosenfeld, M.G., Lunyak, V.V., and Glass, C.K. (2006). Sensors and signals: a coactivator/corepressor/epigenetic code for integrating signal-dependent programs of transcriptional response. Genes Dev. *20*, 1405–1428.

Sauerberg, P., Pettersson, I., Jeppesen, L., Bury, P.S., Mogensen, J.P., Wassermann, K., Brand, C.L., Sturis, J., Woldike, H.F., Fleckner, J., et al. (2002). Novel tricyclic-alpha-alkyloxyphenylpropionic acids: dual PPARalpha/gamma agonists with hypolipidemic and antidiabetic activity. J. Med. Chem. *45*, 789–804.

Shi, Z., Resing, K.A., and Ahn, N.G. (2006). Networks for the allosteric control of protein kinases. Curr. Opin. Struct. Biol. *16*, 686–692.

Shiau, A.K., Barstad, D., Loria, P.M., Cheng, L., Kushner, P.J., Agard, D.A., and Greene, G.L. (1998). The structural basis of estrogen receptor/coactivator recognition and the antagonism of this interaction by tamoxifen. Cell *95*, 927–937.

Stols, L., Gu, M., Dieckman, L., Raffen, R., Collart, F.R., and Donnelly, M.I. (2002). A new vector for high-throughput, ligation-independent cloning encoding a tobacco etch virus protease cleavage site. Protein Expr. Purif. *25*, 8–15.

Uppenberg, J., Svensson, C., Jaki, M., Bertilsson, G., Jendeberg, L., and Berkenstam, A. (1998). Crystal structure of the ligand binding

domain of the human nuclear receptor PPARgamma. J. Biol. Chem. *273*, 31108–31112.

Yan, X., Broderick, D., Leid, M.E., Schimerlik, M.I., and Deinzer, M.L. (2004). Dynamics and ligand-induced solvent accessibility changes in human retinoid X receptor homodimer determined by hydrogen deuterium exchange and mass spectrometry. Biochemistry *43*, 909–917.

Accession Numbers

The atomic coordinates and structure factors have been deposited as 2Q61 for the SR145-PPARγ complex, 2Q5S for the nTZDpa-PPARγ complex, 2Q5P for the MRL24- PPARγ complex, 2Q59 for the MRL20- PPARγ complex, 2Q6R for the SR147- PPARγ complex, and 2Q6S for the BVT.13- PPARγ complex.